EarthArXiv Coversheet

Andrew Gunn[1,*,†]

[1]Affiliation: School of Earth, Atmosphere & Environment, Monash University, Australia, 3068
[*]Email: a.gunn@monash.edu
[†]Twitter: @_algunn

Formation and reorganization timescales of aeolian landscapes

Andrew Gunn[1,*]
[1]*School of Earth, Atmosphere & Environment, Monash University, Australia, 3068*
[*]*a.gunn@monash.edu*

Landscapes created through sediment transport are shaped by the interaction of flow and form. In landscapes where wind is the agent of geomorphic work, this is clear at the small-scale; equilibrium landform morphology is linked to the wind climate and the supply of sediment. At larger scales, this linkage becomes ambiguous because the form of giant dunes and dune fields integrate long histories of varied wind and sand supply. Without a framework to assess aeolian landscape evolution at this scale, the time taken to form and reorganize these landscapes has been largely unexplored quantitatively. We show that these timescales can be understood by linking modern wind and topographic datasets for one of the most expansive and morphologically diverse dune fields, the Rub' al Khali. By linking sediment flux to the surface area and slope of the mobile landscape, and growth to the divergence in that flux, we fully couple form and flow at the aeolian landscape-scale. Our results show quantitatively how wind-blown landscape formation and reorganization is outpaced by climate change, the scale below-which the landscape can equilibrate with climate, and the implications for stratigraphic interpretation.

INTRODUCTION

At the scale of an individual dune useful theories for the equilibrium morphology and orientation of landforms have been developed (Courrech du Pont et al., 2014; Rubin & Hunter, 1987; Werner & Kocurek, 1997), but as dunes grow, the ability to reorganize to a new wind climate reduces since their surface grows slower than their volume (Gunn et al., 2022a). Where climate has changed, this means that larger dunes may not have morphologies and orientations predictable using these theories, whereas the smaller dunes do (Kocurek & Ewing, 2005; Warren & Allison, 1998). This delineation in scale is often not assessed, and it depends on the timescale over which modern climate has persisted.

Often the stratigraphic record left behind by dunes is used to infer aspects of past climate such as the orientations of winds (e.g., Bray & Stokes, 2003; Preusser et al., 2002; Kocurek & Havholm, 1993). These inferences rely on interpretation of any modification of the lithified sediment, but also of the morphology of dunes and the rates of deposition (Brookfield, 1997; Day & Kocurek, 2017). It is typically assumed that the stratigraphy records the climate at the time of deposition, neglecting the potential for dune disequilibrium with climate.

Previous work addressing the formation of aeolian landscapes generally have two approaches. The first focuses on the concept of sand flows, in which the mean wind pattern transports sand away from a source to form a dune field (Pye & Tsoar, 2008; Lancaster, 1985). This concept considers the divergence in the sand flux only qualitatively. The second approach is to core dune sand and quantify the age and mineralogy of sand, and the time since buried sand was last exposed (e.g., Bray & Stokes,

2003; Goudie et al., 2017). This allows for estimates of accumulation rates and the likely source of sand but it is only a local measurement. Neither consider the total amount of sediment and the rate it is distributed. There have been few theoretical and observational studies that consider these (Kocurek & Havholm, 1993; Wilson, 1971; Chanteloube et al., 2022; Gunn et al., 2020), but none that measure both.

Here we link sediment flux to the surface area and slope of the mobile landscape, and landscape change to flux divergence using the ALOS Global Digital Surface Model (Tadono et al., 2014) and ERA5-Land (Muñoz Sabater, 2019) datasets (1-arcsecond and 0.1-degree horizontal resolution, respectively). We pair this with spatial trends in the morphology and orientation of dunes, and the amount of sand, to quantify the timescales over which modern-day conditions would form and reorganize dunes. We also infer what the deposited stratigraphy would look like and show how to infer deposition rate from cross-bed area.
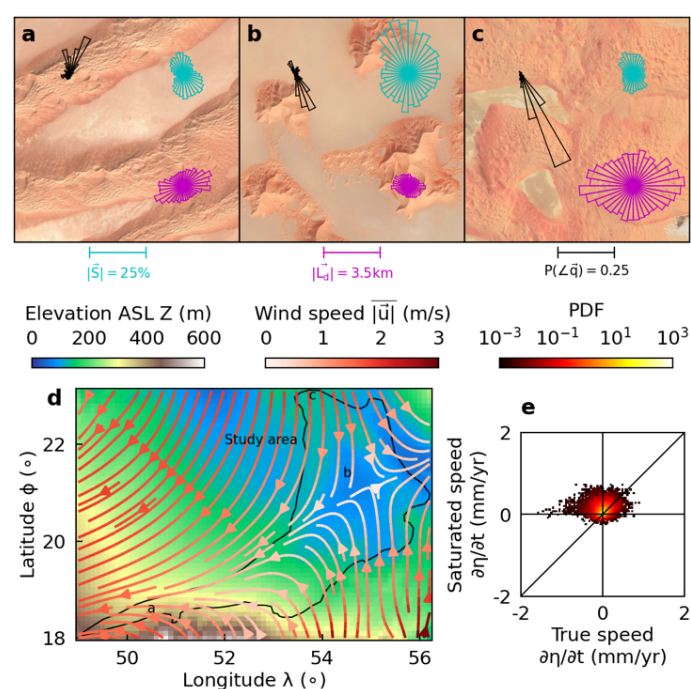

Figure 1: (A) Example transverse dunes overlaid by angular distributions of; top left, sediment flux probability $P(\angle\vec{q})$; top right, dune slope $|\vec{S}|$; bottom right, dune length $|\vec{L_d}|$. Flux probability is defined in the direction of (not direction from) flux. Length and slope are defined in the direction wind encounters them from. As (A) for (B) star and (C) barchanoid dunes. Scales are given below (A-C), locations annotated in (D), all images 4-km across. (D) Elevation above sea-level Z of the study area (outlined in black) overlaid by a stream-plot of average winds over the region, colored by speed. (E) Joint probability density function of monthly elevation change $\partial\eta/\partial t$ at each grid-point calculated using true (x-axis) or saturated (y-axis) flux.

RESULTS

We start by measuring the state of the landscape by calculating key metrics of shape and scale using the topography data (Supplemental Material[1]). The mean elevation of the dynamic landscape (i.e., "equivalent thickness"; Wasson & Hyde, 1983) across a region are found owing to the partially exposed substrate below the sand, as are the distribution of the dune slope that the wind encounters and the length of the dune the wind passes over in a given direction (Fig. 1A–C, S1). These are calculated on tiles centered on the wind reanalysis grid

points to attaining the true sediment flux. The true sediment flux is found by scaling the saturated flux (inferred from hourly 1981-2020 reanalysis winds) by the wind-facing slope and the amount of dynamic landscape it passes over (Courrech du Pont et al., 2014; Kocurek & Lancaster, 1999). In the example locations in Figure 1, these distributions of slope, length and flux are consistent with the dune morphology.
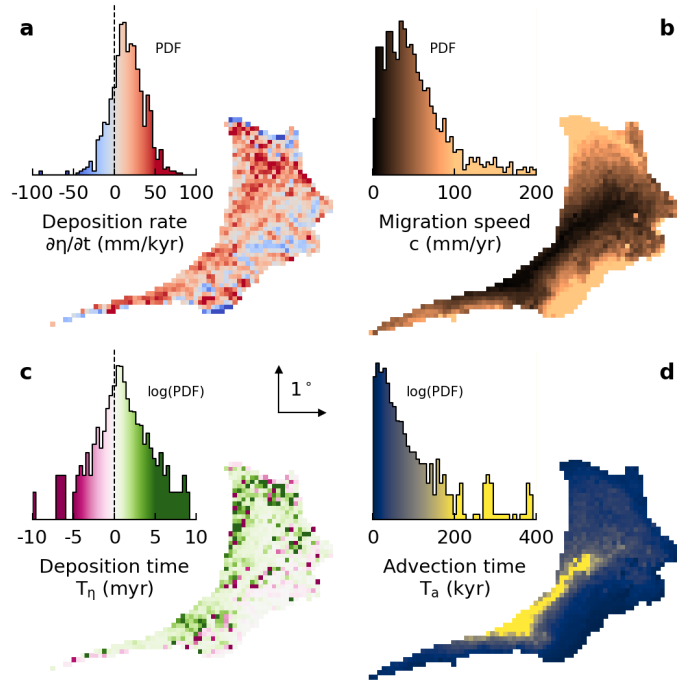
Figure 2: (A) Distribution and map of deposition rate. Equivalent to (A) for; (B) dune migration speed c, (C) Deposition time T_η, and (D) Advection time T_a. Dashed lines in (A) and (C) density functions delineate erosion (left) and deposition (right). Density function y-axes are linear in (A) and (B), and logarithmic in (C) and (D). All maps share the coordinate scale in the center. Color bars embedded in density functions (colors saturate at half the absolute x-axes bounds).

Spatial trends in landform morphology are driven by heterogeneity in wind climatology and sand supply. Shamal winds transport sediment from the north into the study area, and a saddle point is produced in the average wind field where they meet the monsoon winds from the south (e.g., Preusser et al., 2002; Fig. 1D). Sediment is sourced in the northwest from the wider dune field, and from alluvium bounding the dune field in the south (Garzanti et al., 2017; Fig. 1D). There is debate as to what extent deposition rates from these sources have varied over the Holocene (Bray & Stokes, 2003; Goudie et al., 2000), but we find that overall, the region is primed for landscape formation: wind blows inward where supply exists and slows toward the saddle point to create deposition. The shamal and monsoon winds are persistent features of regional paleoclimate but where they meet, and their respective strengths, has likely varied (Garzanti et al., 2017).

We can assess the way the landscape redistributes material within itself by calculating the divergence in flux (Supplemental Material). We find that the area is net depositional, but also that rates of deposition and erosion in the study area are dramatically different when calculated using saturated or true flux (Fig. 1E). This is due to landscape properties (Gunn et al., 2020); largest differences occur where winds slow downwind, but dunes become steeper (Fig. S2), or they cover more surface. The modern landscape shows clear deposition in the northwest, with erosion on the fringes and where the flow sees strong positive gradients in dune steepness (Fig. 2A). These vertical changes occur with horizontal advection of landforms (i.e., dune migration), which is inferred from their height and transport through them (Rubin & Hunter, 1982; Fig. 2B, Supplemental Material).

To attain timescales of formation and reorganization of the landscape, we can divide characteristic lengths by these speeds. The deposition time T_η is the elevation η over the deposition rate $\partial \eta / \partial t$; positive values indicate how long the modern system would take to deposit the amount of existing sand, whereas negative values imply how long it would take to remove the existing sand. The advection time T_a is the time it would take the modern system to migrate a dune its length $\overrightarrow{L_d}$ in the net flux direction; this is the time all the material in a 'Ship of Theseus' landform is reorganized (i.e., "bedform reconstitution time"; Hajek & Straub, 2017). The deposition time T_η (~1 myr) is around two decades larger than the advection time T_a (~10 kyr), which is expected from a scaling analysis (Supplemental Material) and measured estimates (Stokes & Bray, 2005; Goudie et al., 2000), however both vary with the confluence of wind and landscape patterns.

The ability to reconcile landscape morphology from climate and sediment supply, and the inverse, is a key problem in geomorphology (e.g., Passalacqua et al., 2015; Ewing et al., 2015). For this purpose, phase diagrams spanned by key metrics pairing climate and supply have been developed (Fig. 3A,D). Wasson & Hyde (1983) first defined which morphology to expect given supply, measured as average sand thickness (i.e., η), and wind climate, measured as the ratio of the net saturated sand flux vector magnitude over the summed length of all saturated sand flux vectors (i.e., the saturated flux directionality $\hat{q_s}$ or "RDP/DP"). We find that many Rub' al Khali dunes do not adhere to this original diagram (Fig. 3A). Another perspective comes from Rubin & Hunter (1987) and Courrech du Pont et al. (2014); dunes with sufficient supply have crests perpendicular to the net true flux direction, whereas those starved of sediment are parallel. Again, many dunes in the study area do not adhere to this classification (Fig. 3D).

Limiting attainable system information influences our ability to classify morphology and hence understand landscapes. We consider rudimentary knowledge of topography (planform only, Fig. 3B) or winds (saturated flux only, Fig. 3C), or higher-order knowledge (3-dimensional topography, Fig. 3E; true flux, Fig. 3F). Some discernible trends in morphology reveal themselves in these plots, particularly when identifying morphology from the shallowest wind-facing slope and elevation (Fig. 3E). The similar lack of ability to classify the study area landforms using well-adopted theories versus using simple and incomplete information might lead us to call for their revision, however we believe the root cause is the landscape's disequilibrium with respect to climate and supply. Clear examples of this disequilibrium are barchan dunes and dome dunes proximal to star dunes. The largest bedforms in Fig. 3G appear as barchans, however their crests are sinuous like star dunes and across smaller
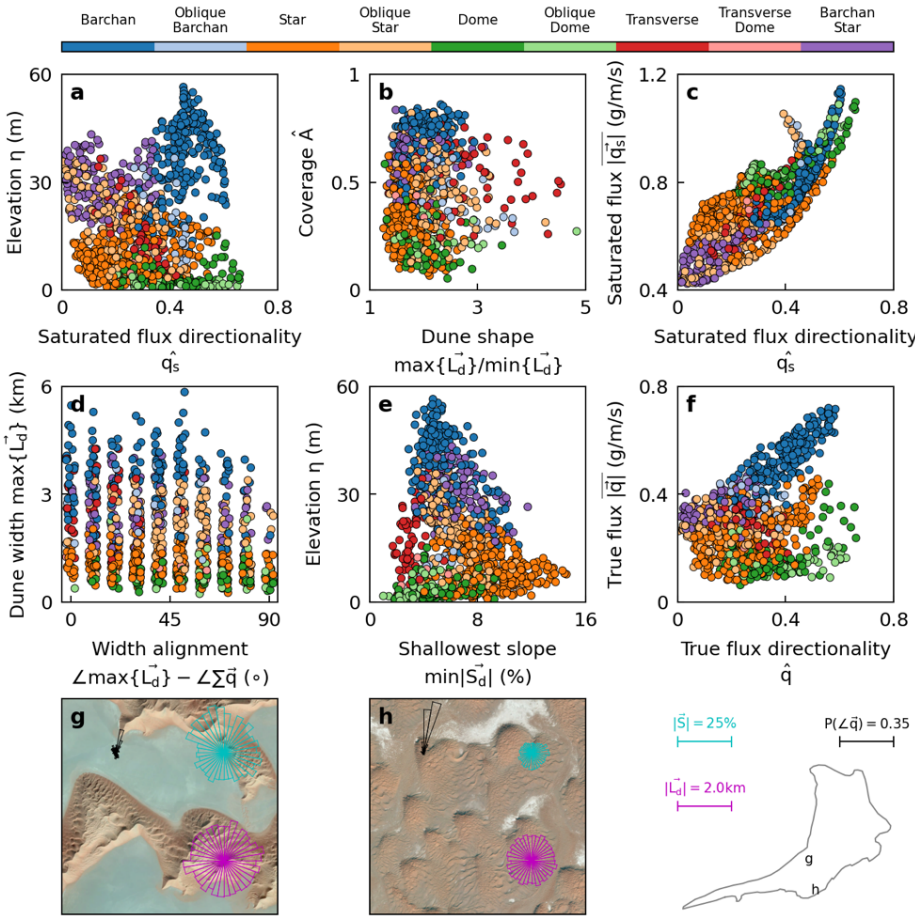
Figure 3: (A) Saturated flux directionality $\hat{q}_s$ vs. elevation η. (B) Ratio of the longest $max\{\overrightarrow{L_d}\}$ and shortest $min\{\overrightarrow{L_d}\}$ planform dune length vs. fraction of surface covered by dunes $\hat{A}$. (C) Saturated flux directionality $\hat{q}_s$ vs. average saturated flux magnitude $\overline{|\vec{q_s}|}$. (D) Smallest angle between net true flux direction $\sum_t \vec{q}$ and longest planform dune length $max\{\overrightarrow{L_d}\}$ vs. $max\{\overrightarrow{L_d}\}$. (E) Shallowest wind-facing dune slope $min|\vec{S}|$ vs. η. (F) True flux directionality $\hat{q}$ vs. average true flux magnitude $\overline{|\vec{q}|}$. Markers represent one 0.1-degree grid tile, colored by morphological category (labels on color bar). (G) Example out-of-equilibrium barchans overlaid by distributions defined as in Fig. 1. As (G) for (H) out-of-equilibrium dome dunes. Scales are given below (A-C), locations annotated in (D), all images 4-km across.

scales the bedforms have varied orientations. The true flux direction distribution is dispersed with a dominant mode almost opposite to the expectation for barchans. In Fig. 3H, we see a contrasting example where the largest dunes in the area have uniform angular morphologies, yet all smaller bedforms consistently have crests perpendicular to the unimodal true flux direction.

How can we quantify this disequilibrium? To what extent does it influence our ability to infer climate and supply from stratigraphy created by dunes, if dunes do not accurately represent their forcing? We attempt to answer these questions by revisiting T_η and T_a, but first we must define a timescale of climate persistence T_c. This is the amount of time climate remained in a state where the probability distribution of sand flux directions remained reasonably consistent. If the ratio of the advection time over the climate persistence time T_a/T_c, which we call here the Memory number, is less than unity this implies dunes completely reorganise during a consistent climate regime and hence have equilibrium morphologies. When the Memory number is greater than unity, the landscape is reorganizing slower than the climate, and it retains a memory of the previous climate.

Accessing T_c is not simple and it is itself a spatial field. Consider the saddle point in the study area's wind field moving northward with a reduced strength of the shamal winds: T_c would only reduce in the saddle's vicinity, not everywhere. To conceptualise how T_a/T_c operates, we use the misalignment between the directions of the steepest wind-facing dune slope and the net true flux (Fig. 4C, S2).

For all morphologies present in the study area, their steepest face should be opposite the net flux. No dunes with Memory numbers below unity should exist without this misalignment, and those that do are out of

equilibrium. Without access to T_c, we plot T_a against this misalignment (Fig. 4D). Whereas the most misaligned dunes are those that morphologically appear in equilibrium, and those more aligned are out of equilibrium, T_a alone cannot recover the expectation for the Memory number, implying that T_c is heterogenous in the study area. We can also define the Mobility number as the ratio T_η/T_a (Jerolmack & Mohrig, 2007). When its magnitude is large, landforms are very mobile—they migrate very fast relative to the speed they are created or destroyed. We compare this number to η and find a scattered positive trend for equilibrium dunes (as apparent through morphology): surprisingly the landscape is thickest where it is most mobile (Fig. 4B).

By comparing the Mobility and Memory numbers, we can understand how past climate is preserved in the stratigraphic record (Fig. 4E). When Mobility is negative the landscape erodes—no stratigraphy is preserved—and it is unlikely to be less than unity (Supplemental Material). Smaller positive values indicate a highly depositional system, where bedforms are encoded into stratigraphy efficiently (Hajek & Straub, 2017). When small positive values of Mobility occur when the Memory number is less than unity, that stratigraphic signature represents the climate. This region of the phase diagram is where stratigraphic interpretation is reliable (shaded green in Fig. 3E). Very few Rub' al Khali dunes with low mobility are both in equilibrium with the climate and will have interpretable stratigraphy. In the most interpretable case of a unidirectional dune with a slip face, we can infer what the stratigraphy itself should look like. The set thickness δ is the product of the dune length and the slope made by the migration speed and the deposition rate (Brookfield, 1997), while the cross-bedding width ε is the product of the migration speed and the timescale over which a bed is
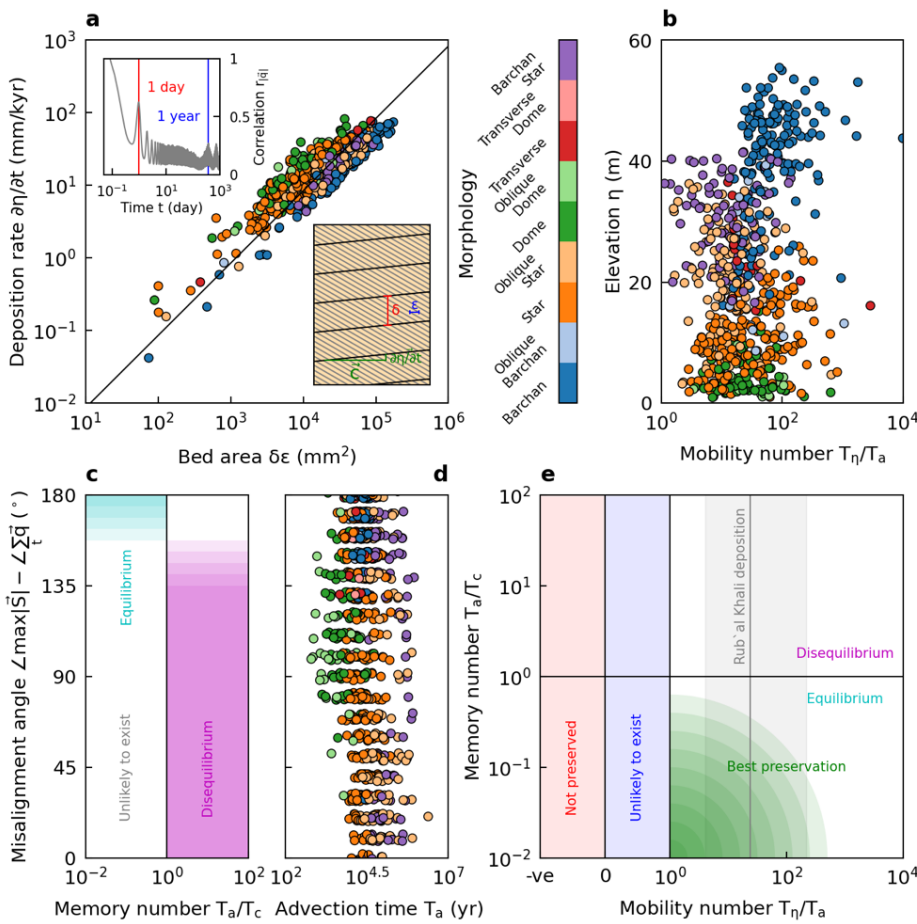
Figure 4: (A) Calculated area of stratigraphic beds, i.e., product of the cross-bedding width ε and set thickness δ (shown in bottom left inset), vs. deposition rate $\partial\eta/\partial t$. ε calculated using annual timescale (top right inset). Best-fit line shown, spread is due to variations in dune size. (B) Mobility number T_η/T_a (ratio of deposition and advection timescales) vs. average elevation η for aggrading regions. (C) Conceptual diagram of dune equilibrium based on Memory number T_a/T_c and difference in angle between the steepest face of a dune $max|\vec{S}|$ and resultant sediment flux $\sum_t \vec{q}$; regions labelled. As (C) for (D) the study site but not scaled by the unknown T_c. (E) Conceptual diagram of stratigraphic preservation and climate inference, spanned by Mobility and Memory numbers, regions labelled. 5th and 95th percentile range (grey band) and median (grey line) Mobility numbers in the case study's aggrading regions, respectively. Markers colored by morphological category (labels on color bar).

made (Supplemental Material; Fig. 4A schematic inset). While cross-beds have a range of widths, the most periodic discernible width is the one associated with the annual timescale (Supplemental Material; Fig. 4A plot inset). Figure 4A shows that the inferred product of these length-scales—bed area when viewed in a strike-normal section—and deposition rate are correlated.

DISCUSSION

In landscapes shaped by water, the coupling between hydrology and topography is essential in their development; basins route flow and macroscopic landscape change cannot be predicted by precipitation alone (Passalacqua et al., 2015). Here we illustrate the analogy holds in landscapes shaped by wind. The interaction between the largest-scale topography and winds is necessary to understand their development. Often aeolian transport is assessed with winds independent of topography using saturated flux; we have shown that Rub' al Khali dune morphology cannot be understood with that approach and suggest the same is true in general.

There is a clear need to identify the climate persistence timescale T_c to test the implications of this study. We suggest T_c can be inferred in the modern by finding the maximum length $\vec{L_c}$ in an area of interest of bedforms that have morphologies consistent with the observed wind climate (Gunn et al., 2022b), where $\vec{L_c}$ is in the direction of net true flux. Then with that bedform's height and the flux, its migration speed c can be inferred and a minimum bound on T_c is $\vec{L_c}/c$.

REFERENCES CITED

Bray, H. E., & Stokes, S. (2003). Chronologies for Late Quaternary barchan dune reactivation in the southeastern Arabian Peninsula. *Quaternary Science Reviews*, 22(10-13), 1027-1033.

Brookfield, M. E. (1977). The origin of bounding surfaces in ancient aeolian sandstones. *Sedimentology*, 24(3), 303-332.

Chanteloube, C., et al. (2022). Source-to-sink aeolian fluxes from arid landscape dynamics in the Lut Desert. *Geophysical Research Letters*, 49(4), e2021GL097342.

Courrech du Pont, S., Narteau, C., & Gao, X. (2014). Two modes for dune orientation. *Geology*, 42(9), 743-746.

Day, M., & Kocurek, G. (2017). Aeolian dune interactions preserved in the ancient rock record. *Sedimentary Geology*, 358, 187-196.

Ewing, R. C., Hayes, A. G., & Lucas, A. (2015). Sand dune patterns on Titan controlled by long-term climate cycles. *Nature Geoscience*, 8(1), 15-19.

Garzanti, E., et al. (2017). Tracing transcontinental sand transport: From Anatolia–Zagros to the Rub'Al Khali Sand Sea. *Journal of Sedimentary Research*, 87(11), 1196-1213.

Goudie, A. S., et al. (2000). Latest Pleistocene and Holocene dune construction at the north-eastern edge of the Rub Al Khali, United Arab Emirates. *Sedimentology*, 47(5), 1011-1021.

Gunn, A., et al. (2020). Macroscopic flow disequilibrium over aeolian dune fields. *Geophysical Research Letters*, 47(18), e2020GL088773.

Gunn, A., et al. (2022a). What sets aeolian dune height? *Nature communications*, 13(1), 1-8.

Gunn, A., East, A., & Jerolmack, D. J. (2022b). 21st-century stagnation in sand-sea activity. *Nature Communications*.

Hajek, E. A., & Straub, K. M. (2017). Autogenic sedimentation in clastic stratigraphy. *Annual Review of Earth and Planetary Sciences*, 45, 681-709.

Jerolmack, D. J., & Mohrig. D. (2007). Conditions for branching in depositional rivers. *Geology 35.5*: 463-466.

Kocurek, G., & Ewing, R. C. (2005). Aeolian dune field self-organization–implications for the formation of simple versus complex dune-field patterns. *Geomorphology*, 72(1-4), 94-105.

Kocurek, G., & Havholm, K. G. (1993). Eolian Sequence Stratigraphy – A Conceptual Framework: Chapter 16: Recent Developments in

Siliciclastic Sequence Stratigraphy.

Kocurek, G., & Lancaster, N. (1999). Aeolian system sediment state: theory and Mojave Desert Kelso dune field example. *Sedimentology*, *46*(3), 505-515.

Lancaster, N. (1985). Winds and sand movements in the Namib sand sea. *Earth Surface Processes and Landforms*, *10*(6), 607-619.

Muñoz Sabater, J. (2019). ERA5-Land hourly data from 1981 to present. *Copernicus Climate Change Service (C3S) Climate Data Store (CDS)*, *10*.

Passalacqua, P., et al. (2015). Analyzing high resolution topography for advancing the understanding of mass and energy transfer through landscapes: A review. *Earth-Science Reviews*, *148*, 174-193.

Preusser, F., Radies, D., & Matter, A. (2002). A 160,000-year record of dune development and atmospheric circulation in Southern Arabia. *Science*, *296*(5575), 2018-2020.

Pye, K., & Tsoar, H. (2008). *Aeolian sand and sand dunes.* Springer Science & Business Media.

Rubin, D. M., & Hunter, R. E. (1987). Bedform alignment in directionally varying flows. *Science*, *237*(4812), 276-278.

Rubin, D. M., & Hunter, R. E. (1982). Bedform climbing in theory and nature. *Sedimentology*, *29*(1), 121-138.

Stokes, S., & Bray, H. E. (2005). Late Pleistocene eolian history of the Liwa region, Arabian Peninsula. *Geological Society of America Bulletin*, *117*(11-12), 1466-1480.

Tadono, T., et al. (2014). Precise global DEM generation by ALOS PRISM. *ISPRS Annals of the Photogrammetry, Remote Sensing and Spatial Information Sciences*, *2*(4), 71.

Warren, A., & Allison, D. (1998). The palaeoenvironmental significance of dune size hierarchies. *Palaeogeography, Palaeoclimatology, Palaeoecology,* 137(3-4), 289-303.

Wasson, R. J., & Hyde, R. (1983). Factors determining desert dune type. *Nature*, *304*(5924), 337-339.

Werner, B. T., & Kocurek, G. (1997). Bed-form dynamics: Does the tail wag the dog? *Geology,* 25(9), 771-774.

Wilson, I. G. (1971). Desert sandflow basins and a model for the development of ergs. *Geographical Journal*, 180-199.

METHODS

Topographic analysis—We employ the ALOS Global Digital Surface Model to study topography (Tadono et al., 2014). This data is at 1-arcsecond horizontal resolution and 1-m vertical resolution. The full topography field was split into tiles centered on the wind data grid points, which is at 0.1-degree horizontal resolution, so each topographic tile is 360 grid-points long in each dimension. We focus only on the 1,047 tiles in the landscape where bedrock is exposed between the dunes in order to estimate the dune volume. For each of these tiles, we identify the dune volume and area coverage, and for a given wind angle, the average length flux occurs over, the average slope the wind sees, and the average length of dunes (Fig. S1).

To calculate these quantities, we need to mask out the exposed bedrock. We do this by first taking the absolute local slope at all grid points on the tile and applying a median filter disk with diameter of 10 arcseconds to it. We define all places on the landscape as bedrock where the values of this field are below a threshold, except the places where the absolute elevation there is one standard deviation of all the tile's topography above the median absolute elevation of the below-threshold-slope topography. This exception needs to be included as some dunes have quite flat surface and would be considered bedrock otherwise. We then mask out all the bedrock to calculate the properties of the dunes (Fig. S1).

The area of dune coverage A_b is simply the summed area of grid points in the tile not considered bedrock. The area fraction $\hat{A}$ is the dune coverage area over the area of the tile A, $\hat{A} = A_b/A$. The dune volume V_b is calculated by looking at cross-sections of the masked topography with constant latitude and integrating the area between the topographic profile of the dune segments and the minimum elevation in the segment. These areas are then integrated across latitude to find volume. The equivalent thickness η is V_b/A (Wasson & Hyde, 1983; Fig. S2), and the average dune height H_b is $\eta/\hat{A}$.

For the wind direction dependent quantities, we first produce equally spaced cross-sections of the topography at that angle with increasing distance defined in the wind direction. The length of dune surface in that direction $\overrightarrow{L_b}$ is defined as the average proportion of these cross-sections including dune topography multiplied by the tile length L. The average wind-facing slope for the tile $\overrightarrow{S_d}$ is defined as the slope from the base of the dune to its peak along the cross-section, weighted by the slope lengths. The average dune length $\overrightarrow{L_d}$ is defined as the average proportion of the cross-section any given dune covers multiplied by the tile length. This process is conducted for 10-degree bins of wind directions.

Sediment flux calculation—We first employ the ECMWF ERA5-Land climate reanalysis from 1981 to 2020 (inclusive; Muñoz Sabater, 2019) to compute the saturated sediment flux from the wind field. ERA5-Land data is currently provided at 0.1-degree horizontal resolution and 1-hour time resolution. We take the 10-m altitude wind vector field $\overrightarrow{u_{10}}$ and calculate the surface friction velocity using the Law of the Wall, $\overrightarrow{u_*} = \overrightarrow{u_{10}} \kappa/ln (10/z_0)$, where Von Karman's constant is $\kappa = 0.4$ and the roughness length is $z_0 = 10^{-3}$ m. This surface friction velocity field is then used to calculate sediment flux in excess of a threshold friction velocity for sand transport. The threshold is defined as $u_{cr} = \alpha\sqrt{gd\left(\rho_s - \rho_f\right)/\rho_f}$ after Bagnold (1941), where the dimensionless constant of proportionality is $\alpha = 0.082$, gravity is $g = 9.8$ m/s², sediment diameter is $d = 0.3$ mm, sediment density is $\rho_s = 2650$ kg/m³, and fluid density is $\rho_f = 1.2$ kg/m³. This gives $u_{cr} = 0.21$ m/s. We use these representative constants in lieu of more precise values for the Rub' al Khali. Saturated sediment flux is then defined in the direction of above-threshold winds as $\overrightarrow{q_s} = \gamma\,\rho_f u_{cr}\left(\overrightarrow{u_*} - u_{cr}\right)^2/g$ after Martin & Kok (2017), where the dimensionless constant of proportionality is $\gamma = 5$.

This saturated sediment flux is then adapted using the topographic quantities described above to find the true sediment flux $\vec{q}$. The average true sediment flux across the dune is half the saturated sediment flux at the brink $\overrightarrow{q_{s,br}}$ because flux increases from zero at the dune foot to the brink flux at the brink, then decreases to zero at the toe. This neglects the slip-face, but in our study site most dunes do not have well-defined slip faces. The saturated sediment flux at the brink is higher than the saturated sediment flux because the wind speeds up in proportion to the slope of the dune the wind sees $\overrightarrow{S_d}$. We define $\overrightarrow{q_{s,b}} = \overrightarrow{q_s}$) after Courrech du Pont et al. (2014), where the dimensionless value $\beta = 9.44$. We have chosen this value for β such that the average value of $\beta\overrightarrow{S_d} = 1$ for the study site, in accordance with numerous observations and theoretical results for the speed-up of winds hills and dunes (Courrech du Pont et al., 2014; Pugh, 1997; Jackson & Hunt, 1975). The true sediment flux is therefore $\overrightarrow{q_{s,br}}/2$ scaled by the proportion of dune surface seen from that direction, $\vec{q} = \overrightarrow{q_{s,br}}\overrightarrow{L_b}/2\,L$. This approach assumes

that topography is quasi-static over the duration of the computed fluxes; a reasonable assumption since the average distance dunes migrate over 40 years is ~0.02% of the horizontal resolution of the wind data.

Sediment flux analysis—We use the true sediment flux field $\vec{q}(x, y, t)$ found using the method outlined above to compute the rate of elevation change $\partial \eta / \partial t$ and metrics for the true flux like the net flux and the flux directionality (i.e., "RDP/DP"). The rate of elevation change is defined using the Exner equation (Bagnold, 1941; Exner, 1925). $\partial \eta / \partial t = -(\partial \vec{q} / \partial x + \partial \vec{q} / \partial y) / \phi \rho_s$, where the packing fraction is $\phi = 0.6$. In practice this is produced on an offset grid from the $\vec{q}(x, y)$ field because it is defined between the flux vectors, then it is interpolated back onto the same grid as $\vec{q}(x, y)$. The net flux $\overrightarrow{q_{net}}$ is defined as the sum of the true flux divided by the duration of observation T, $\overrightarrow{q_{net}} = \sum_t \vec{q} / T$. The flux directionality $\acute{q}$ is the ratio of the length of the net flux vector over the length of all flux vectors, $\acute{q} = |\sum_t \vec{q}| / \sum_t |\vec{q}|$.

Timescale scaling analysis—The deposition timescale T_η is defined as $\eta / (\partial \eta / \partial t)$, and the advection timescale T_c is defined as $\overrightarrow{L_d} / c$ where $\overrightarrow{L_d}$ is in the direction of net true flux. The deposition rate is $\partial \eta / \partial t = -(\partial \vec{q} / \partial x + \partial \vec{q} / \partial y) / \phi \rho_s$, and the migration speed is $c = |\vec{q}| / (H_b \phi \rho_s)$. These variables are defined in the methods sections above. We can infer the relative scale of these timescales by taking their ratio, the Mobility number (Jerolmack & Mohrig, 2007), and reducing it. By taking these equations we can write $T_\eta / T_a \, \eta q \Delta L / (L_d H_b \Delta q)$. Now first we note that H_b is $\eta / \mathring{A}$, and we define $\hat{L} = L_d / \Delta L$, where ΔL is the discretised distance over which the flux change Δq is measured. $\mathring{A}$ and $\hat{L}$ are less than unity by definition and are approximately equal. We therefore have $T_\eta / T_a \, \mathring{A} q / (\hat{L} \Delta q)$. Since gradients in q aren't larger than its magnitude (strictly positive) and the area and length fractions $\mathring{A}$ and $\hat{L}$ are close, we can say that $T_\eta / T_a \gtrsim 1$.

Stratigraphic analysis—We use dune geometry and sediment flux to infer the set thickness and cross-bedding width preserved in dune stratigraphy (Rubin & Hunter, 1982; Brookfield, 1977). The set incline angle θ_δ is angle made by the deposition rate over the migration speed (Brookfield, 1977), $tan \theta_\delta = \partial \eta / \partial t / c$, and the set thickness δ is the height made by this angle across the dune length (Rubin & Hunter, 1982; Brookfield, 1977), $\delta = L_d \partial \eta / \partial t / c$. The cross-bedding width ε is the product of the migration speed and the time a bed is made. We take this timescale to be the most powerful timescale of transport, the annual cycle, so $\varepsilon = c T_a$. These values lose meaning where the flux directionality is low and are most applicable in unidirectional depositional regime (Rubin & Hunter, 1982). When taking the product of the set thickness and the cross-bedding width, the migration

speed c cancels.

Study site characterization—We focus on the region in the Rub' al Khali where there is bedrock exposure so that we can measure the active landscape thickness η. We found this area using Landsat imagery on Google Earth and drew a perimeter around it that was used to mask the wind and topography data. To the northwest, the perimeter delineates the boundary between dunes with and without interdune exposure. To the southeast, the perimeter delineates the edge of the dune field. We manually identified the typical morphology of the largest dunes within each of the 1,047 0.1-degree wide tiles centered on the gridded wind data points within this perimeter (Fig. S2). This typical morphology was categorized using standard nomenclature.

DATA AVAILABILITY
The ERA5-Land reanalysis data used in this study are available in the Climate Data Store database https://cds.climate.copernicus.eu/. The ALOS Global Digital Surface Model data used in this study are available in the OpenTopography database https://opentopography.org.

CODE AVAILABILITY
Code to reproduce this paper can be found at https://github.com/geomorphlab/fluxdiv.

METHODS REFERENCES CITED

Bagnold, R. A. (1941). *The physics of blown sand and desert dunes*. Courier Corporation.

Brookfield, M. E. (1977). The origin of bounding surfaces in ancient aeolian sandstones. *Sedimentology*, 24(3), 303-332.

Courrech du Pont, S., Narteau, C., & Gao, X. (2014). Two modes for dune orientation. *Geology*, 42(9), 743-746.

Exner, F. M. (1925). Über die wechselwirkung zwischen wasser und geschiebe in flüssen. *Akad. Wiss. Wien Math. Naturwiss. Klasse*, 134(2a), 165-204.

Jackson, P. S., & Hunt, J. C. R. (1975). Turbulent wind flow over a low hill. *Quarterly Journal of the Royal Meteorological Society*, 101(430), 929-955.

Jerolmack, D. J., & Mohrig. D. (2007). Conditions for branching in depositional rivers. *Geology* 35.5: 463-466.

Martin, R. L., & Kok, J. F. (2017). Wind-invariant saltation heights imply linear scaling of aeolian saltation flux with shear stress. *Science advances*, 3(6), e1602569.

Muñoz Sabater, J. (2019). ERA5-Land hourly data from 1981 to present. *Copernicus Climate Change Service (C3S) Climate Data Store (CDS)*, 10.

Pugh, J. M. (1997). *The quaternary desert sediments of the Al Liwa area, Abu Dhabi*. University of Aberdeen (United Kingdom).

Rubin, D. M., & Hunter, R. E. (1982). Bedform climbing in theory and nature. *Sedimentology*, 29(1), 121-138.

Tadono, T., et al. (2014). Precise global DEM generation by ALOS PRISM. *ISPRS Annals of the Photogrammetry, Remote Sensing and Spatial Information Sciences*, 2(4), 71.
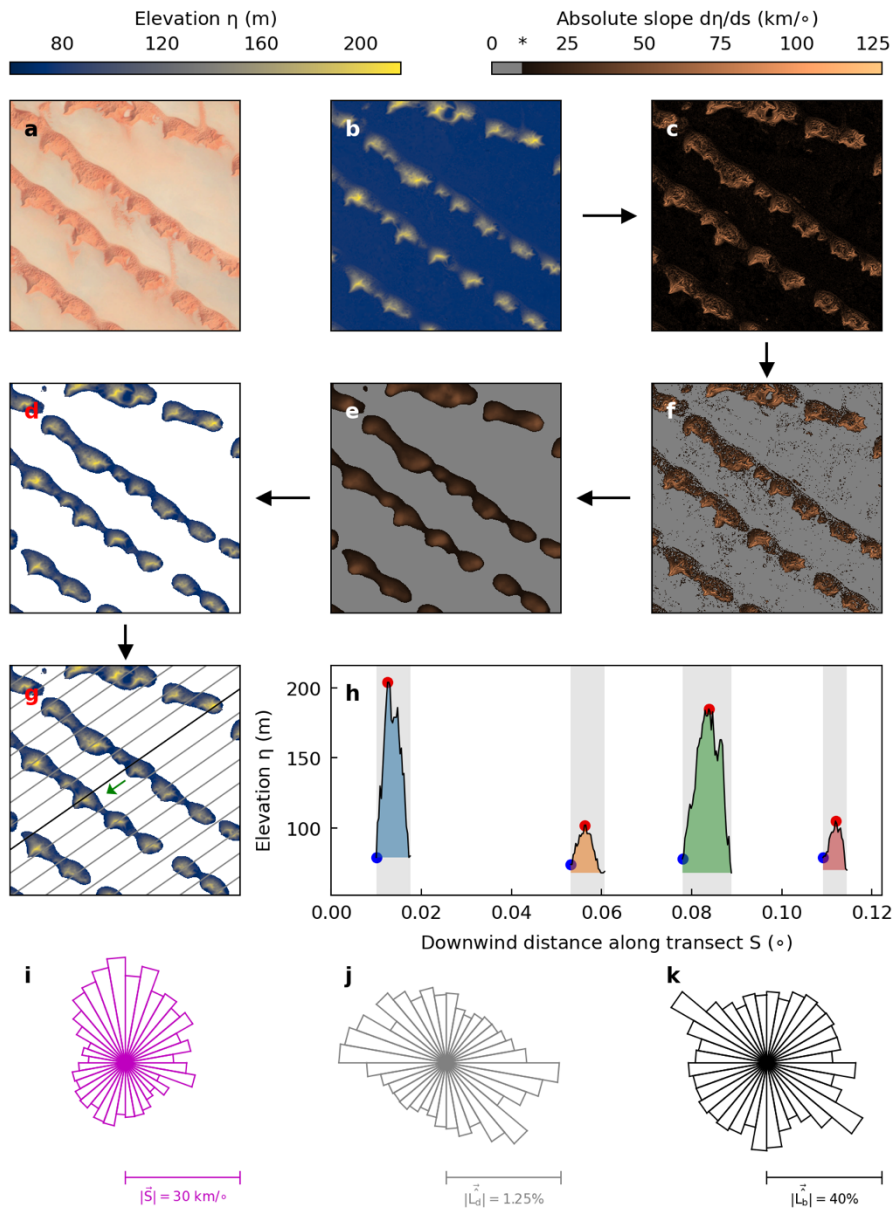
Figure S1: Topography analysis. (a) Satellite imagery of example tile. (b) The elevation map of the example tile from ALOS Global Digital Surface Model; this is centered on an ERA5-Land grid point and has the same width and height as the grid spacing. (c) The maximum absolute slope of the surface from (b). (f) The same as (c) but all values less than a threshold (marked with an asterisk in the color bar) are shaded grey. (e) The output of (f) with at 10-arcsecond median filter disk applied to find areas consistently flat; the non-grey area is considered the area fraction of the dunes. (f) The original topography in (b) with the grey area of (e) masked out; this is considered the dune topography. (g) Transects for directional properties across (d) in in grey with one example transect in black. The green arrow marks the direction of the transects. (h) The elevation profile along the example black transect in (g), the transect x-axis increases in the direction of the transect. The black lines indicate the dune topography. The shaded area beneath the dunes is bounded by their respective heights and minimum elevations; this is how dune volume is calculated. The grey shaded areas behind the dunes represent their length coverage of the transect. The blue dots indicate the base of the wind-facing slope, whereas the red dots indicate the maximum height of the wind-facing slope. (i) The distribution of average (weighted by the slope lengths) wind-facing slope for this tile across all angles. (j) The distribution of the proportion of transects covered by dunes (average fraction width of grey shaded areas in (h) for all transects, across all angles. (k) The same as (j) but the sum of the grey shaded areas. Scales for the distributions (i-k) are given below each and are defined in the direction a wind encounters them from. Color bar for (b,d,g) in top left; for (c,e,f) in top right. Imagery by Maxar via Google Earth.
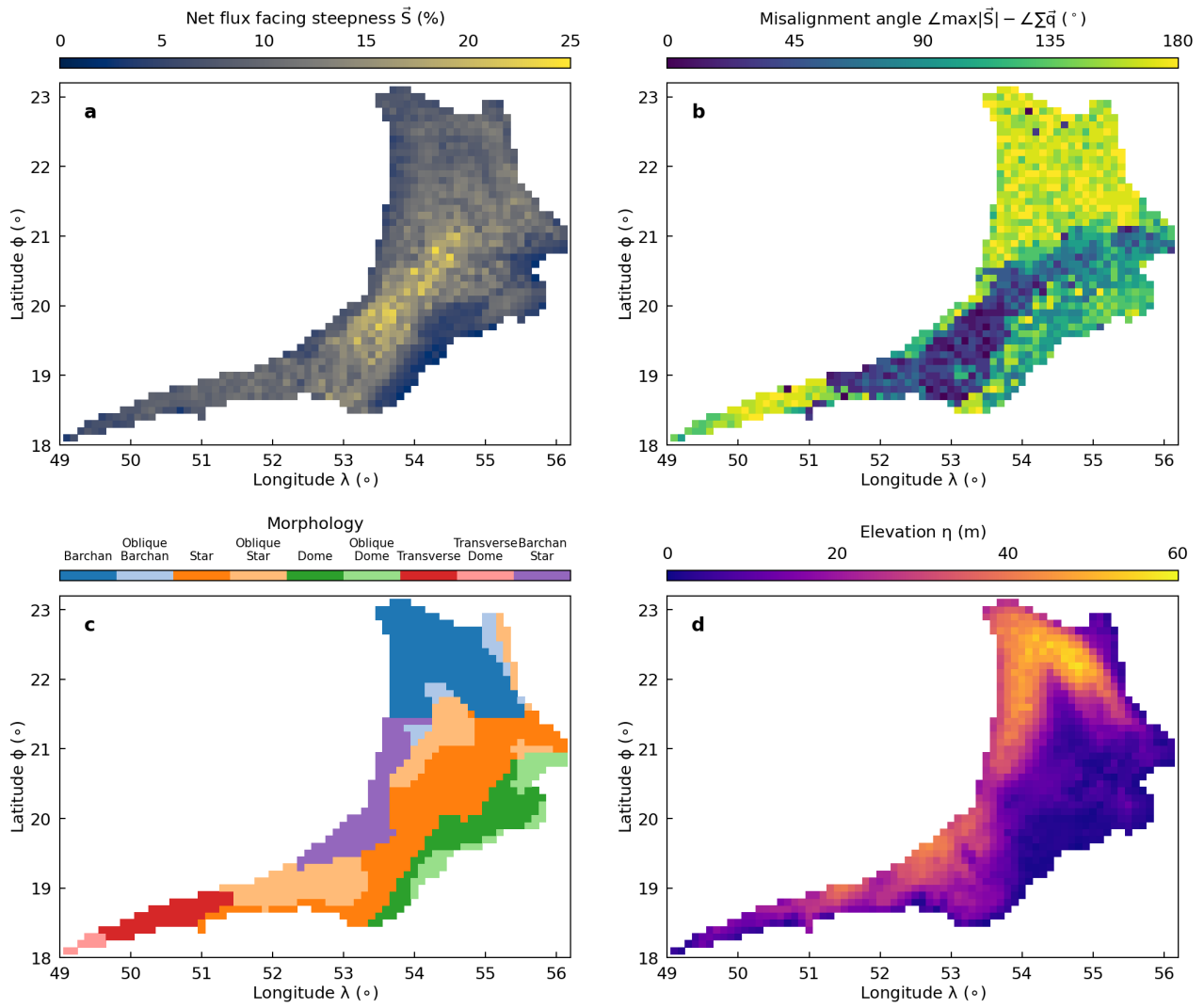
Figure S2: Maps of study area properties. (a) The slope of the landscape facing the net true flux direction. (b) The smallest angle between the steepest slope of the landscape and the net true flux direction. (c) The manually classified morphology. (d) The elevation of the dynamic landscape, i.e., "equivalent thickness".